ACS Catalysis

pubs.acs.org/acscatalysis
Research Article

Mechanism of Two-Component Mono-Oxygenases Involved in Anthracycline 1-Hydroxylation

Benjamin Nji Wandi, Pedro Dinis, Vilja Siitonen, Gunter Schneider, Robert Schnell,* and Mikko Metsä-Ketelä*

Cite This: *ACS Catal.* 2024, 14, 12359−12371
Read Online

ABSTRACT: Anthracyclines are microbial natural products with important antiproliferative bioactivities that are widely used in anticancer chemotherapy. Several anthracyclines, including nogalamycin and kosinostatin, contain a 1-hydroxyl group, which is installed by an atypical two-component mono-oxygenase system. Here, we clarify the structural and mechanistic basis for 1-hydroxylation. We present the crystal structure of the NADPH-dependent reductase SwaQ2 in complex with doxorubicin, which indicates that the reaction is initiated by quinone reduction. The reduced anthracycline ligand may react with molecular oxygen, leading to the formation of a peroxide intermediate similar to flavin chemistry. The structures of the polyketide cyclase-like SnoaL2, involved in nogalamycin biosynthesis, in complex with substrate and product reveal a novel catalytic tetrad, which is used to stabilize a reduced reaction intermediate to direct the reaction toward 1-hydroxylation. Furthermore, we report the characterization of several unknown anthracycline 1-hydroxylases, which display varied substrate profiles. The structure of polyketide cyclase-like KstA15 from the kosinostatin pathway enabled structure-based protein engineering to expand the substrate specificity of the enzyme to include glycosylated anthracyclines. Our work provides insight into how reductase-hydroxylase two-component systems circumvent the need for organic cofactors or metal ions to catalyze monooxygenations in several anthracycline pathways.

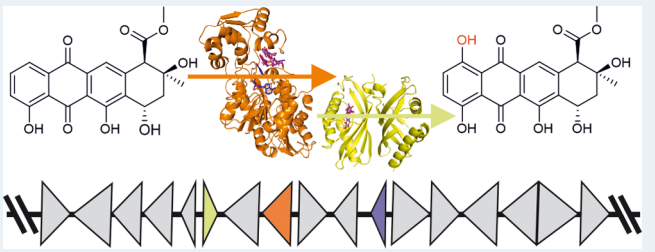

KEYWORDS: *enzyme mechanism, mono-oxygenase, short-chain alcohol dehydrogenase/reductase, natural product, biosynthesis*

INTRODUCTION

Anthracyclines are microbial natural products produced by Actinobacteria, predominantly by various Gram-positive *Streptomyces* species.[1] Initially discovered for their biological activity against *Staphylococcus aureus*, anthracyclines are also known for their potent anticancer properties. Chemically, anthracyclines are defined as linear tetracyclic 7,8,9,10-tetrahydro-5,12-naphtacenoquinones decorated with one or more carbohydrate units.[2] Daunorubicin (**1**) and doxorubicin (**2**) are widely used anthracyclines, which serve as first-choice chemotherapy agents for treating both solid and hematological tumors (Figure 1a).[3] Aclacinomycin A is currently prescribed in Japan and China for acute myeloid leukemia.[1] The success of **2** as an antiproliferative agent has led to the discovery of a large family of over 500 naturally occurring anthracyclines.[4] Additionally, thousands of semisynthetic anthracyclines have been screened to enhance their biological activity, resulting in the discovery of six clinically important drugs.[1]

Despite 50 years of investigation, the biological activities and the pharmaceutical potential of anthracyclines are not fully elucidated.[5] All anthracyclines bind to DNA in a similar manner, with the polyphenolic anthracyclinone aglycone intercalating between DNA bases, while the carbohydrate unit at C7 enhances binding affinity by positioning itself in the minor groove of DNA. The biological effects induced by the anthracycline-DNA complex vary and depend on the structure of the anthracycline, but the two key outcomes are topoisomerase poisoning[6] and histone eviction.[7] Despite their success in cancer chemotherapy, **1** and **2** are associated with severe treatment-limiting side effects such as cumulative cardiotoxicity.[5] In contrast, aclacinomycin A and the semisynthetic *N,N*-dimethyl-doxorubicin have recently been shown to lack cardiotoxicity,[8] renewing interest in the development of novel anthracycline congeners.

Anthracyclines belong to aromatic type II polyketides, and their carbon scaffold is biosynthesized from acetyl-CoA or propionyl-CoA starter unit via nine rounds of iterative Claisen condensations with malonyl-CoA.[2] Cyclization and aromatization of the decaketide by a conserved set of enzymes lead to the formation of the archetypical four-ring anthracyclinone. The great diversity of anthracyclines is generated in tailoring steps,

Received: May 8, 2024
Revised: July 19, 2024
Accepted: July 22, 2024

https://doi.org/10.1021/acscatal.4c02623
ACS Catal. 2024, 14, 12359−12371

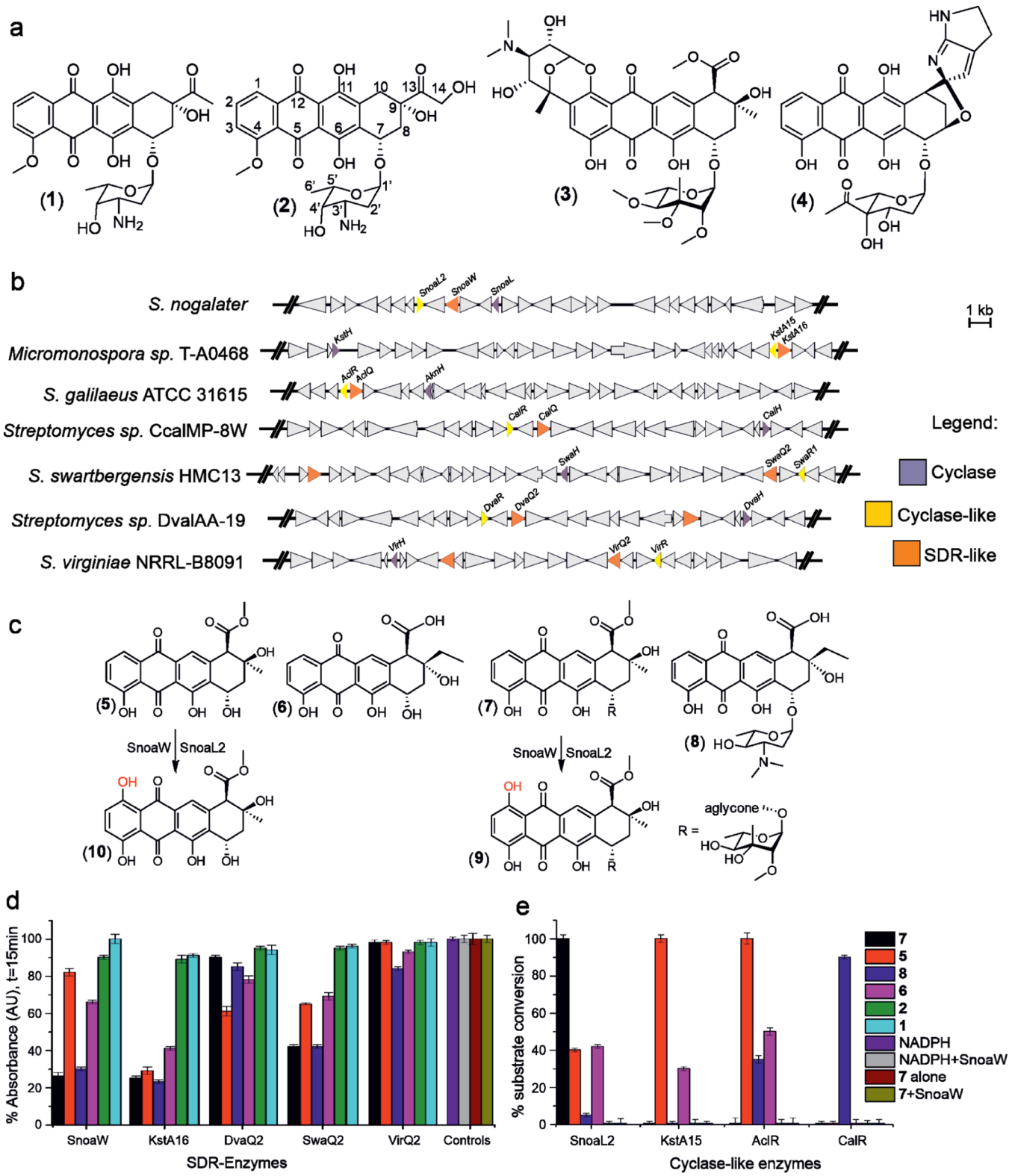

Figure 1. Characterization of anthracycline 1-hydroxylases. (a) Chemical structures of daunorubicin (**1**), doxorubicin (**2**), nogalamycin (**3**), and kosinostatin (**4**). (b) Genome mining identifies anthracycline BGCs encoding proteins homologous to SnoaW and SnoaL2. (c) Chemical structures of additional substrates nogalamycinone (**5**), aklavinone (**6**), 3′,4′−demethoxy-nogalose-nogalamycinone (**7**), and aclacinomycin T (**8**) used in this study. Previous studies have confirmed that SnoaW/SnoaL2 convert **5** and **7** to 1−hydroxy-nogalamycinone (**10**) and 3′,4′−demethoxy-nogalose-1-hydroxy-nogalamycinone (**9**), respectively. The site of 1-hydroxylation is shown in red. (d) The substrate promiscuity of SDR-enzymes showing NADPH-dependent reduction of anthracycline substrates. Relative activities of the enzymes were investigated via consumption of NADPH, which was monitored at 340 nm by UV/vis spectrophotometry.[18] (e) Enzymatic assay of the cyclase-like enzymes in partnership with SnoaW. Substrate conversion was monitored by HPLC (Figure S3). The activity measurements were carried out in triplicate with standard deviation shown as errors bars.

https://doi.org/10.1021/acscatal.4c02623
ACS Catal. 2024, 14, 12359−12371

where various redox or group transfer reactions modify the common carbon scaffold. Glycosylation with diverse amino- or neutral deoxysugars is an important factor for the biological activity of anthracyclines.[9]

Numerous anthracycline biosynthetic gene clusters (BGCs) encode redox enzymes belonging to various protein families, which highlight the importance of molecular oxygen in the chemo-diversification of anthracyclines.[1] However, the producing organisms face challenges as reactions between natural products and O_2 are limited by kinetic and thermodynamic barriers,[10] rendering molecular oxygen mostly inert under ambient conditions. In order to harness the use of O_2 in biochemistry, nature has evolved several classes of enzymes that utilize organic cofactors such as flavin or transition metals to break the spin barrier-limiting reactivity.[11] Examples of classical mono-oxygenases or oxidases involved in anthracycline biosynthesis include flavoenzymes such as the 11-hydroxylase RdmE residing on the rhodomycin pathway,[12] the cytochrome P450 enzyme DoxA responsible for several oxidations in daunorubicin biosynthesis,[13] the 2-oxoketoglutarate and nonheme iron-dependent carbocyclase SnoK,[14] and the Rieske mono-oxygenase SnoT[15] involved in nogalamycin (**3**) biosynthesis (Figure 1a).

In addition to classical redox enzymes, many anthracycline biosynthetic pathways include mechanistically intriguing cofactor-independent mono-oxygenases such as the quinone-forming antibiotic biosynthesis mono-oxygenase (ABM) SnoaB,[16] methyltransferase-like 10-hydroxylase RdmB,[17] and, pertinent to this study, a two-component 1-hydroxylase system SnoaW and SnoaL2.[18] A common feature of these enzymes is that the enzymes activate the substrate for reaction with the molecular oxygen cosubstrate to aid catalysis in the absence of redox cofactors.[19] Detailed studies have suggested that SnoaB accelerates rate-limiting electron transfer from an anionic substrate to O_2 by decreasing the required reorganization energy.[20] In case of RdmB, the reaction is initiated by 10-decarboxylation of the substrate that leads to the formation of a carbanion intermediate that may react with O_2.[21] The mechanism of 1-hydroxylation has been proposed to resemble flavin chemistry and proceed via initial NAD(P)H-dependent quinone reduction of the anthracyclinone by the atypical short-chain alcohol dehydrogenase/reductase (SDR) SnoaW.[18] Hydride (H−) transfer to the quinone allows activation of the substrate and the formation of an anthracycline—molecular oxygen-caged radical pair that is resolved into a peroxide intermediate. Protonation of the peroxide by SnoaL2,[22] which is structurally similar to anthracycline fourth ring cyclases such as SnoaL,[23] has been suggested to complete 1-hydroxylation.

Here, we provide structural evidence for the mechanism of anthracycline 1-hydroxylation. We characterized several novel and known 1-hydroxylase systems and demonstrated their wide substrate preference. We present the crystal structures of the SDR-type reductase SwaQ2 and the cyclase-like SnoaL2 in complex with ligands, allowing us to explore structure−function relationships and gain insight into catalysis. In addition, the structure of KstA15 from the kosinostatin (**4**) pathway,[24] which is homologous to SnoaL2, facilitated identification of residues important for substrate recognition, which we utilized in engineering of KstA15 to expand its substrate scope. The work provides an extensive new molecular insight into how nature has evolved ingenious ways to utilize O_2 in enzyme catalysis in the absence of organic cofactors or metal ions.

RESULTS AND DISCUSSION

Genome Mining and Characterization of Anthracycline 1-Hydroxylases. We initiated the study by probing sequence databases using the nogalamycin fourth-ring cyclase SnoaL as a query,[23] which led to the identification of 24 potential anthracycline BGCs. In order to pinpoint potential 1-hydroxylases, we searched for the presence of 1-hydroxylase SnoaW/SnoaL2 pairs using MultiGeneBlast,[25] which returned two known BGCs involved in aclacinomycin (AclQ/AclR)[26] and kosinostatin (KstA15/KstA16)[24] biosynthesis. In addition, several unknown BGCs were identified that harbored different combinations and copy numbers of the two genes (Figure 1b). Three BGCs of unknown function were from *Streptomyces* sp. DvalAA-19, *S. swartbergensis* HMC13, and *S. virginiae* NRRL B-8091, each harboring two copies of SDR genes. Phylogenetic analysis indicated that the proteins denoted as DvaQ2, SwaQ2, and VirQ2, respectively, clustering together with SnoaW, were likely to be involved in 1-hydroxylation (Figure S1a). The anthracycline BGC that resides in *Streptomyces* sp. CcalMP-8W contained a single SDR enzyme coding for CalQ. In a similar fashion, phylogenetic analysis was used to resolve SnoaL2-type sequences from polyketide cyclases, which resulted in the discovery of four proteins of unknown function DvaR, SwaR1, VirR, and CalR (Figure S1b).

Next we produced and purified hexahistidine-tagged recombinant SDR and cyclase-like proteins in *Escherichia coli*. Five SDR proteins were purified, and the substrate promiscuity of these enzymes was probed using nonglycosylated anthracyclinones nogalamycinone (**5**) and aklavinone (**6**), the neutral glycoside 3′,4′−demethoxy-nogalose-nogalamycinone (**7**), and three aminoglycosides aclacinomycin T (**8**), **1**, and **2** as substrates (Figure 1a and 1c). Enzyme activity was detected spectrophotometrically in the presence of NADPH by measuring conversion of NADPH to $NADP^+$ at 340 nm. The relative kinetic data indicated that SnoaW preferred neutral glycoside **7** and aminoglycoside **8**, while moderate reduction of aglycones was also observed (Figure 1d). SwaQ2 harbored a similar activity profile to SnoaW, with additional minor activity toward **1** and **2**. KstA16 exhibited broad substrate specificity and was able to reduce both aglycones and glycosylated anthracyclines to their respective dihydroquinones. The activity of DvaQ2 was minor with highest activity detected with aglycones, while VirQ2 only accepted **8** as a substrate, suggesting that VirQ2 is likely to prefer a differently modified anthracycline glycoside as a substrate (Figure 1d and Figure S2). Specific activities are summarized in Table S1.

The activity of the cyclase-like proteins was assayed by HPLC in a coupled reaction with a suitable SDR partner (Figure S3). In general, the substrate specificity appeared to be more stringent than those of the SDR components. The neutral glycoside **7** was the preferred substrate of SnoaL2, although the enzyme was also able to hydroxylate aglycones **5** and **6** (Figure 1e). Surprisingly, only minor activity was detected with aminoglycoside **8**. The activity of AclR mirrored that of SnoaL2 with activity detected with aglycones but a preference for aminoglycoside **8** instead of the neutral glycoside **7**. KstA15 only accepted nonglycosylated aglycones **5** and **6** as substrates, while CalR only hydroxylated **8** (Figure 1e).

Structure of the Quinone Reductase SwaQ2 in Complex with $NADP^+$ and 2. In order to obtain a complex structure of an SDR quinone reductase, we focused on SwaQ2 that performed best in preliminary crystallization trials. We took

https://doi.org/10.1021/acscatal.4c02623
ACS Catal. 2024, 14, 12359−12371

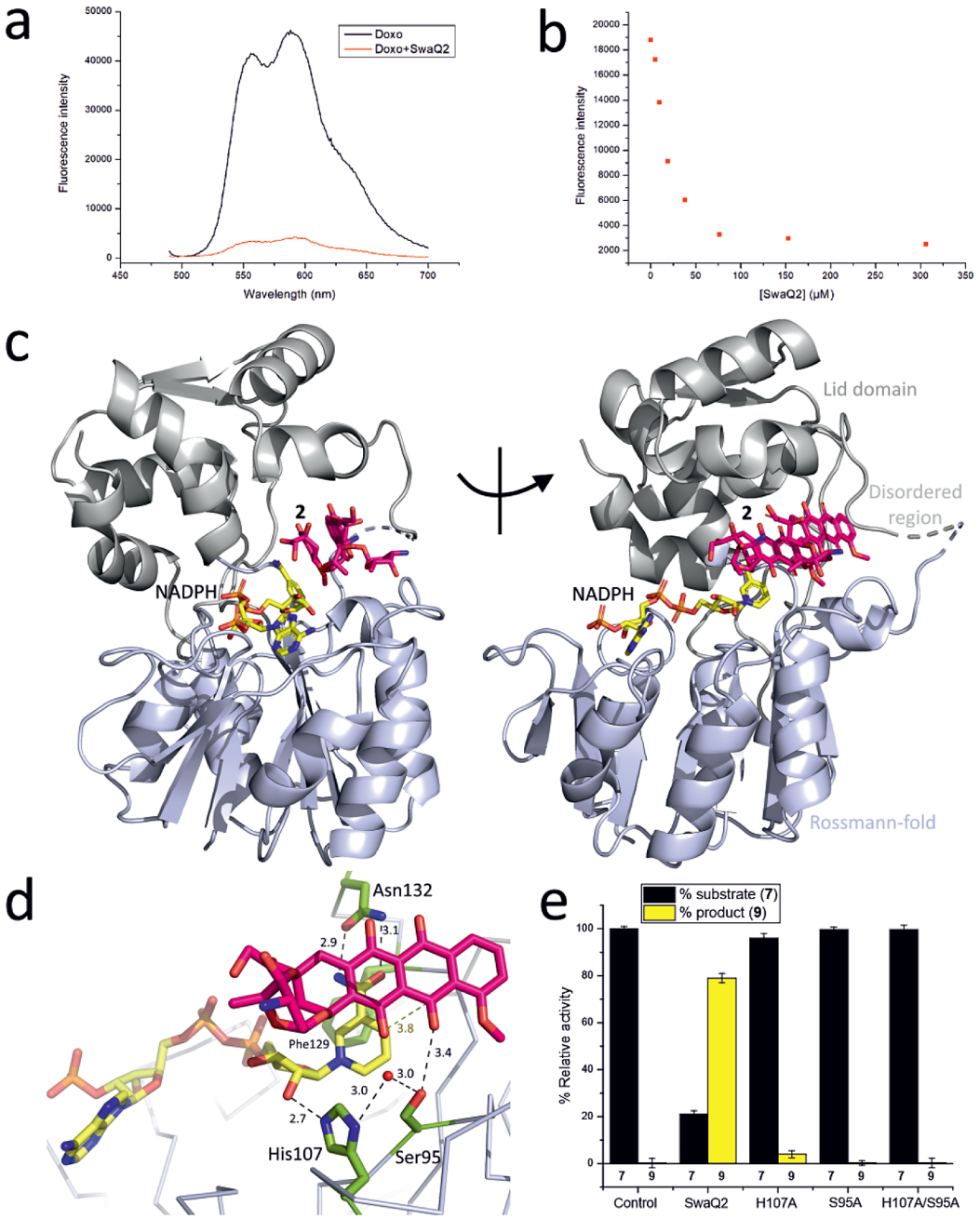

Figure 2. Structural and functional characterization of SwaQ2. (a) Fluorescence spectra of **2** in the absence and presence of SwaQ2 using ligand-specific excitation at 470 nm and recording the emission spectra at 490−700 nm. (b) The fluorescence signal of **2** quenches in a concentration-dependent manner upon titration, with SwaQ2 demonstrating ligand binding. The samples were excited at 470 nm, and emission was recorded at 595 nm. (c) The overall structure of SwaQ2 is depicted as a cartoon with the cosubstrate NADPH as yellow sticks and two molecules of **2** in magenta. Two different orientations of the enzyme are shown to indicate the parallel arrangement of the two ligand molecules. The two domains and the disordered loop (dashed line) are highlighted. (d) Active site architecture of SwaQ2. Hydrogen bonding interactions formed by the amino acid residues Asn132, Ser95, and His107, the cosubstrate NADPH, and the ligand are shown as dashed lines with distances indicated in Å. The red sphere designates a water molecule within hydrogen bonding distance from His107 and Ser95. (e) Relative activities of SwaQ2, the single mutants SwaQ2 His107Ala and Ser95Ala, and the double mutant His107Ala/Ser95Ala. The enzymatic assays were performed with the substrate analog **7** and NADPH in a coupled assay with the cyclase-like enzyme SnoaL2. The SwaQ2/SnoaL2 reaction resulted in the hydroxylation of **7** to **9** (Figure S3). The activity measurements were carried out in triplicate with standard deviation shown as errors bars.

advantage of the inherent fluorescence signal of anthracyclines to detect interactions and to devise an assay to approximate the binding affinities of the various anthracyclines toward SwaQ2. The fluorescence signal of **2** substantially decreased in the presence of SwaQ2 (Figure 2a), suggesting that binding at the active site altered the fluorescent properties of **2** due to a change in the chemical environment. Moreover, titration with an increasing concentration of SwaQ2 revealed a binding constant K_D in the low micromolar (4.7 ± 1.7 μM) range (Figure 2b and Figure S4).

We crystallized SwaQ2 in the presence of $NADP^+$/NADPH and **2**, and we determined the X-ray structure to 2.4 Å resolution (Table S2). The asymmetric unit of the P65 crystal unit cell contained two monomers that are essentially identical, and

https://doi.org/10.1021/acscatal.4c02623
ACS Catal. 2024, 14, 12359−12371

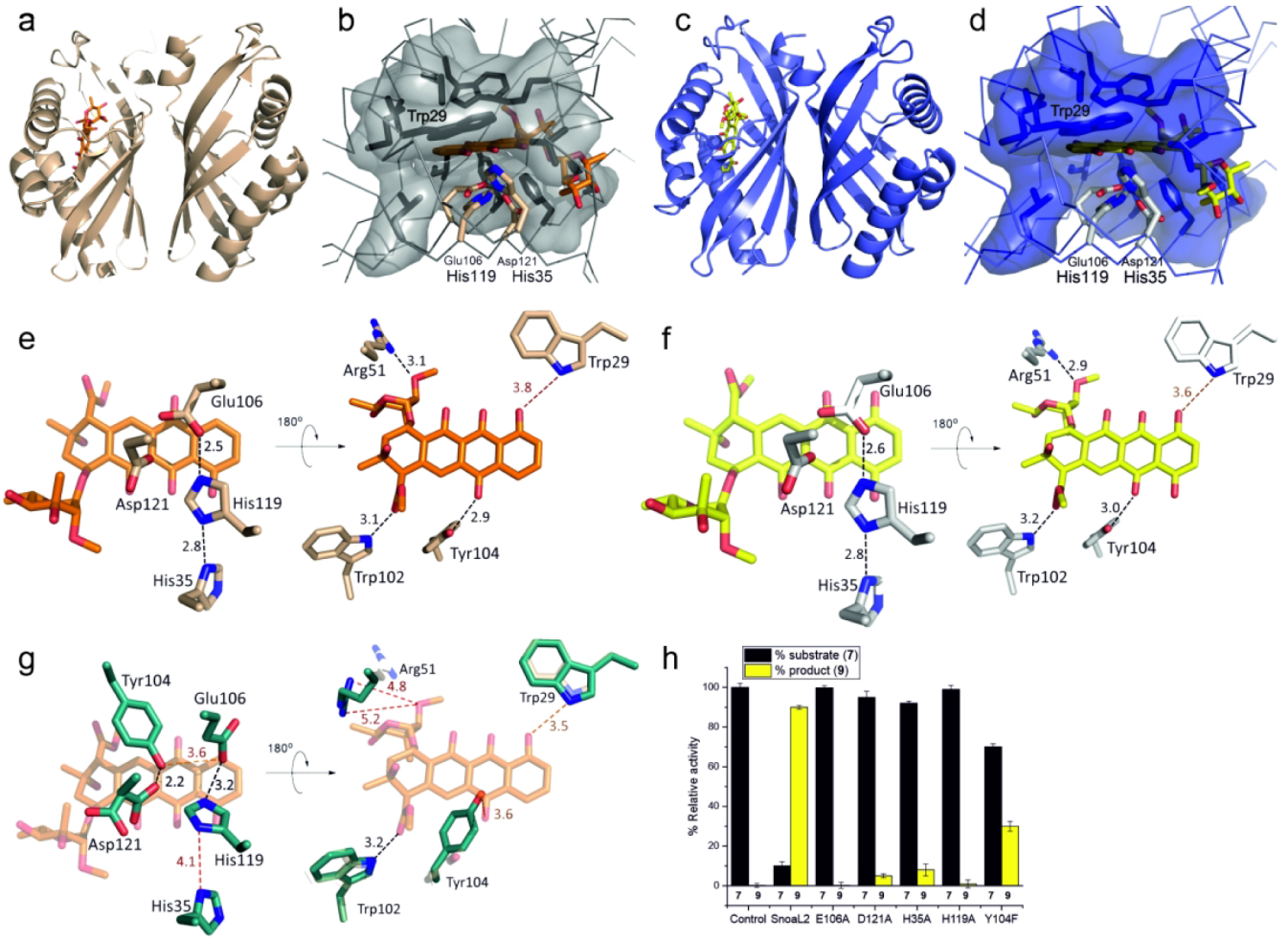

Figure 3. Structural and functional characterization of SnoaL2. The dimer of SnoaL2 in complex with **7** (a, b—beige cartoon; ligand is depicted as a stick model in orange) and **9** (c,d—blue cartoon; ligand is depicted as a stick model in yellow). One side of the active site cavity is composed of a hydrophobic cage formed around the anthracycline ring system of the substrate **7** (b, transparent gray surface representation) and the product **9** (d, transparent blue surface representation). Trp29 is labeled as a reference point. The opposite face of the active site is formed by a patch of hydrophilic residues His35, Glu106, His119, and Asp121 that are depicted as sticks. Hydrogen bonding interactions between SnoaL2 and (e) the substrate **7** and (f) product **9** are shown from two directions rotated by 180°. Hydrogen bonds are depicted as dashed lines with the distances indicated in Å. (g) Comparison of the hydrogen bonding network between the SnoaL2 in complex with **7** (transparent orange) and the ligand-free SnoaL2 structure (dark green). Hydrogen bonds are depicted as dashed lines with the distances indicated in Å. (h) The relative enzymatic activities of SnoaL2 and single mutants SnoaL2 Glu106Ala, Asp121Ala, His35Ala, His119Ala, and Tyr104Phe in partnership with SnoaW. The substrate **7** and reaction product **9** are shown in black and yellow, respectively. The columns represent the mean enzyme activity from triplicate measurements with standard deviation shown as errors bars.

superposition resulted in a C_α-r.m.s.d. of 0.4 Å (on 274 of the total 275 residues). The enzyme is built up of two domains: the Rossmann-fold type NADPH-binding domain typical in the SDR family[27] and a lid domain closing over the active site cleft (Figure 2c). The electron density map allowed the modeling of **2** and $NADP^+$/NADPH molecules in both protein chains. The N-terminal methionine residues and a loop in the lid domain (residue ranges 243−260 and 244−260 in the two chains, respectively) were disordered and could not be modeled. A likely reason for the mobility of the loop region was the presence of two molecules of **2** in each active site, which were bound between the nicotinamide residue and the lid domain. The ligands are arranged in parallel to each other, forming a stacking interaction between the anthracycline rings (Figure 2c). The innermost position represents the likely substrate placement for catalysis, directly neighboring the nicotinamide ring and the conserved residues Ser95 and His107. The positioning of the second outermost ligand on the protein surface with access to bulk solvent may indicate that the second ligand position may be considered as an artifact. This is supported by the analysis of the binding kinetics in the solution state (Figure S4), which fits best to a 1:1 binding stoichiometry.

In the active site, the nicotinamide ring of NADPH is positioned by the side chain of Phe129 that is aligned parallel to the cosubstrate. Potential hydrogen bonds are formed additionally between the amide moiety and the side chain of Asn132 and the 2′-hydroxyl group of the ribose and His107. The hydrogen bonding network of His107 extends to Ser95 via a H_2O molecule (Figure 2d). The inner molecule of **2** is positioned parallel to the cosubstrate with the quinone ring in the vicinity of the nicotinamide ring. The 5-carbonyl oxygen of the anthracycline is 3.4 Å from the oxygen of the Ser95 side chain, while the 4-*pro*-S hydride position of the nicotinamide ring is 3.8 Å from the 5-carbonyl carbon of **2** (Figure 2d).

As a member of the extended family of SDR enzymes,[28] SwaQ2 lacks the Ser-Tyr-Lys catalytic triad of classical SDR

https://doi.org/10.1021/acscatal.4c02623
ACS Catal. 2024, 14, 12359−12371

enzymes and instead hosts a Ser-Ile-His triad similar to the angucycline quinone reductase SimC7.[29] Alanine scanning mutagenesis revealed that SwaQ2 His107Ala retained 5% of the catalytic activity, while SwaQ2 Ser95Ala had no enzymatic activity when **7** was used as a substrate (Figure 2e). The identification of catalytically important residues was further confirmed by the lack of activity in the double mutant (Ser95Ala/His107Ala) of SwaQ2 (Figures 2e and S3).

Structure of the Cyclase-Like SnoaL2 in Complex with Anthracyclines. The ligand-free structure of SnoaL2 has previously been determined, which revealed a $\alpha+\beta$ barrel with a large hydrophobic cavity in the interior of the protein.[22] In order to obtain mechanistic insight, we crystallized SnoaL2 in complex with the substrate (**7**) and the product 3′,4′−demethoxy-nogalose-1-hydroxy-nogalamycinone (**9**) (Figure 1c) and determined their structures by X-ray crystallography to 1.8 and 2.0 Å resolution, respectively (Table S2). The crystal asymmetric units contain a SnoaL2 dimer (Figure 3a) with the dimerization mode identical to earlier ligand-free structures of SnoaL2 and AclR.[22] The models include the residue ranges 2−130 or 2−131, with eight or nine residues at the C-terminal end of the polypeptide chains being disordered. The substrate **7** is bound in one active site cleft, while the second active site of the dimer does not contain a ligand. The same ligand-binding arrangement is observed in the structure of SnoaL2 in complex with the product **9**. SnoaL2 in complex with **7** (Figure 3a,b) and in complex with **9** (Figure 3c,d) exhibited the same overall conformation, and the superposition of the polypeptide chains results in a Cα-r.m.s.d. of 0.1 Å over 129 of 130 amino acid residues.

The binding mode and interactions of both **7** and **9** in the active site cleft are highly similar, the polyketide aglycone groups are situated in the deep, predominantly hydrophobic cleft, while the carbohydrate moieties protrude toward the surface of the protein. The hydrophobic cage surrounding the ligands from one side is built by the side chains of Met13, Val14, Trp17, Val25, Trp29, Val48, Met52, Ile80, Tyr104, Leu108, Phe123, and Phe125, which adopt the same conformations and rotamers when comparing the two ligand-bound structures. Notably, none of the aromatic amino acids form hydrophobic pi-pi stacking interactions with the planar ring system of the anthracycline ligands (Figure 3b,d); Trp29 and Trp102 reside above and below, respectively, of the anthracycline aglycone (Figure 3e,f). Polar contacts between the ligands and the protein are not prevalent, with only three residues Tyr104, Trp102, and Arg51 potentially forming hydrogen bonds (Figure 3e,f).

We observed a potential catalytic tetrad on one side of the polyaromatic ligand. This patch of polar residues His35, Glu106, His119, and Asp121 forms a hydrogen bonding network adjacent to the quinone ring system of both the substrate **7** (Figure 3e) and product **9** (Figure 3f) complexes. It is interesting to note that the hydrogen bonding network is missing in the apo structure, and it appears to be formed upon conformational changes that occur during substrate binding (Figure 3g). First, in the absence of the substrate, Glu106 is positioned in the space occupied by ligand, but the residue is forced closer to Asp121 and His119 in the complex structure. Second, Tyr104 interacts with Asp121 in the apo structure (Figure 3g), but in the complex structure, Tyr104 has rotated and forms a hydrogen bond with the quinone oxygen of the ligand (Figure 3e,f).

The importance of the catalytic tetrad His24-Glu106-His119-Asp121 was confirmed by alanine scanning mutagenesis, which significantly reduced the enzymatic activity with **7** to 0%−8% (Figure 3h) after 5 min of reaction. Furthermore, the catalytic tetrad appears to be conserved within the enzyme family, as illustrated by the multiple sequence alignment (Figure S5). In contrast, Tyr104 was not found to be essential for catalysis since the mutant SnoaL2 Y104F retained 30% of relative enzymatic activity after 5 min with **7** (Figure 3h). If the reaction time was increased to 1h, SnoaL2 Y104F shows 90% of activity, while other mutants displayed activity in the range of 4%−35% (Figure S6).

Structure of KstA15 and Molecular Basis for Substrate Promiscuity. As demonstrated above (Figure 1e), KstA15 displays a higher degree of substrate specificity, exclusively accepting aglycones **5** and **6** as substrates, which is in contrast to SnoaL2 that additionally accepts glycosides **7** and **8** (Figure 1e). In order to understand factors that govern the differences in substrate preference, we determined the apo structure of KstA15 to 2.1 Å resolution (Table S2). The overall structure of KstA15 is highly similar to SnoaL2 with an Cα-rmsd of 0.567 Å over 131 amino acid residues (Figure 4a). However, we observed critical differences in the active sites of KstA15 and SnoaL2 that could explain the differences in substrate utilization. Residues Val48, Tyr104, and Phe123 that shape the active site entrance in SnoaL2 correspond to Met61, Ile117, and Met135 in KstA15 (Figure 4b). In addition, differences may be observed at the entrance to the active site cavity, which is broad in SnoaL2 due to Ile39 and Phe125 (Figure 4c), but restricted by Val25 and Tyr137 in KstA15 (Figure 4d).

In order to modulate the substrate specificity of KstA15, we targeted the three residues Met61, Ile117, and Met135 and exchanged them with those found in SnoaL2. Mutation of single amino acid residues in KstA15 led to the production of a small but measurable amount of **9** (Figure 4e) when **7** was used as a substrate. While no dramatic improvement in the formation of **9** was observed with KstA15 double mutants, the triple mutant KstA15 Met61Val/Ile117Tyr/Met135Phe showed efficient production of **9**, reaching 85% of the SnoaL2 activity (Figure 4e). In addition, the mutant exhibited broad substrate tolerance and retained the ability to utilize aglycone **5** as the substrate with the formation of **10** at 69%. It is noteworthy that of the three residues, only Val48/Met61 is in the direct vicinity of the carbohydrate unit of the substrate, while the other two residues Tyr104/Ile117 and Phe117/Met135 are in close contact with the aglycone unit. These results confirm that the three residues participate in the positioning of various substrates in the active site.

Structural Comparison and Evolutionary Implications of Cyclase and Hydroxylase Enzymes. The structure of SnoaL2 in complex with the product **9** (Figure 5a) allowed us to compare the ligand binding to the canonical anthracycline fourth-ring cyclase SnoaL (Figure 5b). Superposition of the structures (Figure 5c) revealed that the two proteins share significant structural similarity despite low sequence identity of 25% with Cα rmsd of 2.3 Å over 119 of 129 amino acid residues of SnoaL. However, the binding of the anthracycline ligands was found to differ drastically, and the substrate protrudes much deeper in the SnoaL2 active site.

SnoaL harbors a catalytic dyad of Asp121-Gln195 to carry out a fourth-ring cyclization (Figure 5d). It is interesting to note that the same Asp121 residue is part of the catalytic tetrad His35-Glu106-His119-Asp121 identified here to be important for catalysis by SnoaL2. However, Asp121 appears to be the only conserved catalytic amino acid, and other residues in the active

https://doi.org/10.1021/acscatal.4c02623
ACS Catal. 2024, 14, 12359−12371

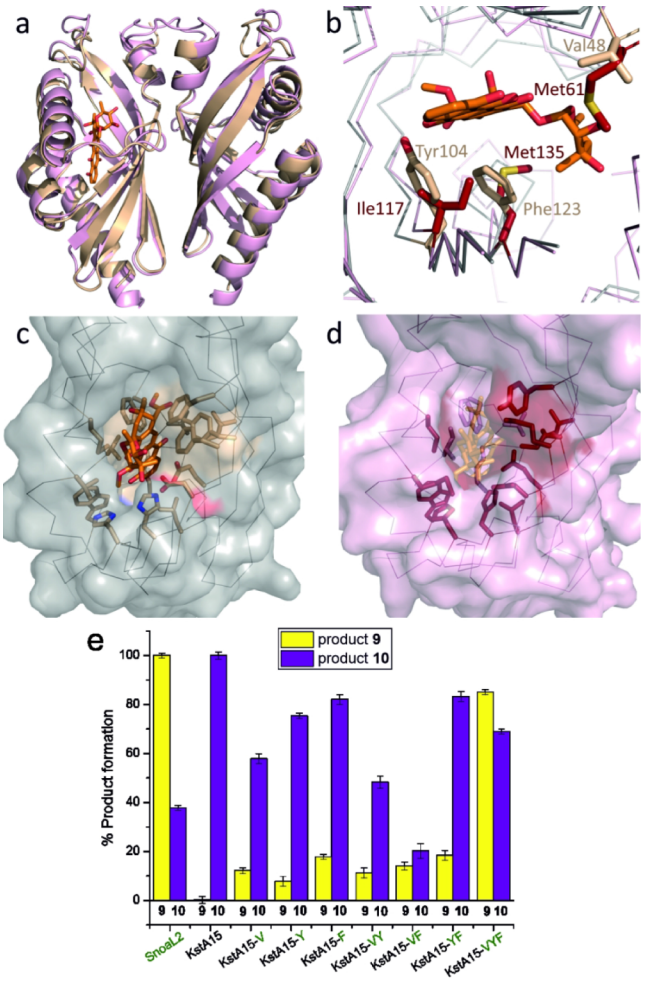

Figure 4. Structural and functional characterization of KstA15. (a) Superimposition of SnoaL2 (beige cartoon) and KstA15 (salmon cartoon) demonstrates similar overall folds. (b) Comparison of the active sites of SnoaL2 (beige sticks; orange ligand) and KstA15 (red sticks) identifies residues responsible for the differences in the size of the active site cavity. The three residues highlighted (Val48, Tyr104, and Phe123 in SnoaL2) are not conserved and are likely responsible for substrate specificity. (c) The wide active site entrance of SnoaL2. (d) The narrow active site entrance of KstA15. (e) Relative enzymatic activities of SnoaL2, KstA15, single mutants (Met61Val, Ile117Tyr, and Met135Phe), double mutants (Met61Val/Ile117Tyr, Met61Val/Met135Phe, and Ile117Tyr/Met135Phe), and the triple mutant (Met61Val/Ile117Tyr/Met135Phe) of KstA15 in partnership with SnoaW. The glycosylated substrate **7** and nonglycosylated substrate **5** were used in the presence of NADPH. The detected reaction products **9** and **10** (Figure 1c) are shown in yellow and purple, respectively. The columns represent the mean values from triplicate measurements with standard deviation shown as errors bars.

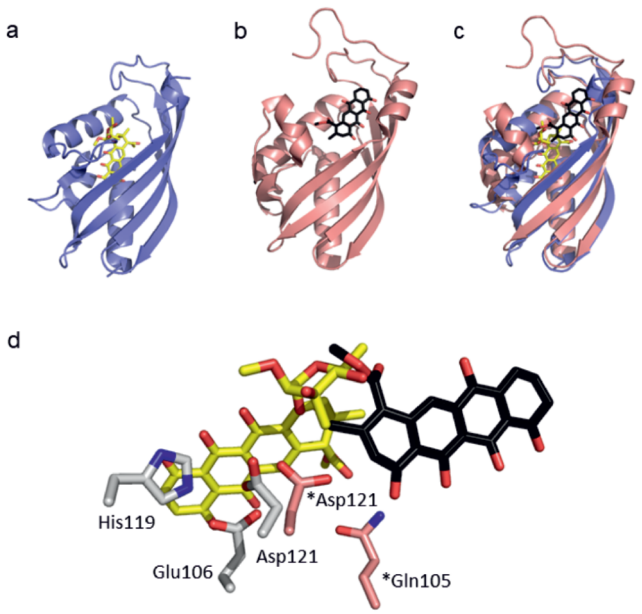

Figure 5. Comparison of ligand binding in the polyketide cyclase SnoaL and the polyketide cyclase-like SnoaL2. (a) SnoaL2 cartoon (blue) with **9** (yellow sticks) bound. (b) SnoaL as pink cartoon with the reaction product (black stick model) bound. (c) The superposition of SnoaL and SnoaL2 with their respective reaction products bound. The fold and overall structure are highly similar, but the ligand position, binding mode, and posture are profoundly different. (d) The residues involved in catalysis are shown in relation to the respective reaction products in yellow and black. *Asp121 and *Gln105 from SnoaL are depicted as sticks with pink carbons. Asp121, Glu106, and His119 from SnoaL2 are depicted as sticks with gray carbons.

sites are poorly conserved to accommodate the different binding modes of the ligands.

Mechanism of 1-Hydroxylation. We propose that the first step in anthracycline 1-hydroxylation is the NADPH-dependent reduction of the quinone unit by SwaQ2. Our structural and functional characterization of SwaQ2 supports a catalytic model, where the reaction of SwaQ2 is initiated by the transfer of a proton directly from Ser95 to the C5 carbonyl group of the anthracycline and is followed by the transfer of the 4-*pro*-S hydride from the cosubstrate NADPH to C5 of the substrate (Figure 2d). This is in contrast to SimC7,[29] where the reaction has been proposed to be substrate assisted and involves intramolecular proton transfer from an adjacent phenolic hydroxyl group to the quinone carbonyl due to retained enzymatic activity in an active site Ser mutant. However, the loss of enzymatic activity in SwaQ2 Ser95Ala (Figures 2e and S3) indicates that anthracycline quinone reduction is more consistent with classical SDR enzymes, where proton transfer from a tyrosine hydroxyl group initiates the reaction. The significantly decreased enzymatic activity in the SwaQ2 His107Ala mutant is in agreement with the critical role of His107 in binding and positioning the cosubstrate via a hydrogen bond to the 2′-hydroxyl of the nicotinamide ribosyl moiety (Figure 2d,e).

The reactivity of anthraquinones with molecular oxygen is well documented and has been the basis of industrial manufacturing of H_2O_2 for several decades.[30] The process is based on chemical reduction of anthraquinones, which is followed by reaction with molecular oxygen, leading to the generation of an anthraquinone peroxide intermediate. Spontaneous cleavage of H_2O_2 simultaneously results in the reformation of the oxidized anthraquinone starting material.[30] In anthracycline 1-hydroxylation, we suggest that the reduced anthracycline reacts with molecular oxygen in the active site of SwaQ2 to ensure the correct regiochemistry. The hypothesis is supported by previous work with SnoaW, indicating that quinone reduction does not occur without the presence of molecular oxygen.[18] In the absence of cyclase-like protein partners, the anthracycline 1-peroxide intermediate is resolved into H_2O_2 and the oxidized anthracycline.[18]

https://doi.org/10.1021/acscatal.4c02623
ACS Catal. 2024, 14, 12359−12371

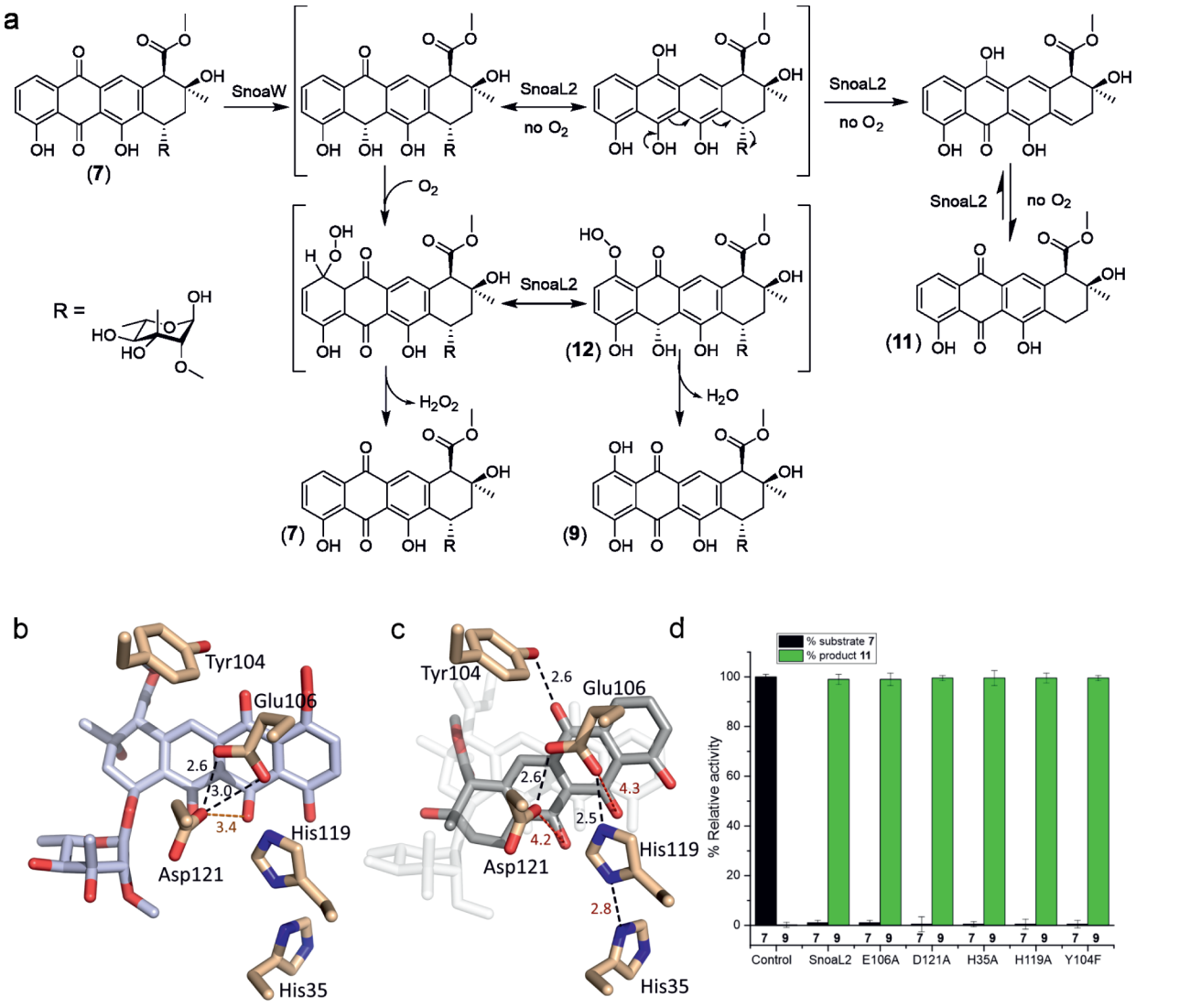

Figure 6. (a) Proposed mechanism of anthracycline C1-hydroxylation and C7-deglycosylation. (b) Modeling of SnoaL2 with the intermediate **12**. (c) Modeling of SnoaL2 with the deglycosylated product **11**. The deglycosylation allows greater flexibility of the substrate within the active site, leading to an ~ 30° rotation of the compound in respect to the position of the glycosylated substrate **7** observed in the crystal structure. Despite the repositioning of compound **11**, the absence of interactions with the catalytic tetrad is similar to that of compound 7 (ghost white). (d) Relative enzymatic activities of WT SnoaL2 and its mutants in partnership with SnoaW under anaerobic conditions. The substrate 7 and reaction product **11** are shown in black and green, respectively. The mass and chemical structure of **11** was confirmed with HR-MS and NMR (Figures S7, S8 and S9). The activity measurements were carried out in triplicate at 293 K for 1 h, and the standard deviation is indicated by the error bars.

We propose that the role of SnoaL2 is to prevent release of H_2O_2 and instead direct the reaction toward 1-hydroxylation. This might be accomplished by stabilizing a resonance form **12** of the substrate that reinforces the aromatic nature of the anthracycline D-ring since cleavage of a phenolic bond between C1 and the proximal oxygen O_p is unlikely. SnoaL2 hosts a novel catalytic tetrad His35-Glu106-His119-Asp121 that is formed upon substrate binding. The three residues Glu106-His119-Asp121 can be observed stacking against the aromatic quinone C-ring of the anthracycline. However, molecular modeling of a resonance structure form of the intermediate **12** (Figure 6b and Table S3), which harbors a reduced quinone with the same C5 stereochemistry as in the product of the SwaQ2 reaction, positions the C5 hydroxyl group toward the hydrogen bonding network of the catalytic triad. We propose that this interaction indirectly stabilizes the C1−O_p bond via D-ring aromatization and allows cleavage of the O_p and distal oxygen O_d bond instead, with concomitant release of H_2O.

Mechanism of Aberrant Anthracycline Deglycosylation. We noted that when the SnoaW/SnoaL2 reactions were carried out in the absence of molecular oxygen using the neutral glycoside **7** as a substrate, a novel product (**11**) was observed by HPLC. The reactions were scaled up, and sufficient material was purified for structure elucidation by NMR (Figures S7, S8 and S9). The experiment revealed that anaerobic conditions in the presence of NAD(P)H led to deglycosylation and the loss of the C7 O-glycosyl group from the substrate (Figure 6a). Formation of an equivalent shunt product has been reported on the kosinostatin pathway when the nonglycosylated **5** was used as a substrate for KstA15 and KstA16 under anoxic conditions.[31]

Here, we demonstrate that SnoaL2 is required for the reaction but that the moonlighting deglycosylation activity differs from the 1-hydroxylation activity. We show that mutation of any of

https://doi.org/10.1021/acscatal.4c02623
ACS Catal. 2024, 14, 12359−12371

the catalytic tetrad residues His35-Glu106-His119-Asp121 does not influence the deglycosylation activity under anoxic condition (Figure 6d). We propose that the mechanism of deglycosylation is similar to the detoxification reactions of anthracyclines by liver P450 enzymes[32] and the cytorhodin self-resistance protein CytA.[33] In a manner similar to that of the flavoprotein CytA, the formation of a reduced dihydroquinone species by SnoaW may undergo C7 deglycosylation to generate a quinone methide, which in turn may rearrange to an oxidized quinone. It is noteworthy that the key intermediate for deglycosylation is a planar dihydroquinone species. Molecular modeling of **11** (Figure 6c and Table S3) indicates that the binding is similar to the glycosylated **7** and the compound does not interact with the catalytic tetrad of SnoaL2 via hydrogen bonding. This provides an explanation for why SnoaL2 mutant enzymes were able to catalyze deglycosylation in comparatively equivalent rates to the wild type (Figure 6d).

CONCLUSIONS

One of the defining features of microbial natural products is their tremendous chemical diversity.[4] In order to achieve this, microbes have evolved to recruit and repurpose enzymes from primary metabolism to catalyze atypical chemical transformations.[34] One mechanistically intriguing class of catalysts that have emerged are metal ion and organic cofactor independent oxidases, which seem to circumvent classical rules for oxygen utilization in biochemistry.[19] Many of these enzymes activate their natural substrates, which are often aromatic in nature, to achieve a reaction between an organic molecule and molecular oxygen.[16,17,19]

Here, we have clarified the structural basis for atypical 1-hydroxylation that occurs on the biosynthetic pathways of several known and unknown anthracyclines. We show that SDR enzymes such as SwaQ2 position the substrates in front of the NAPDH cosubstrate for initial quinone reduction, which leads to formation of an anthracycline carbanion that is able to react with molecular oxygen. The active site of SwaQ2 has a sufficiently large pocket near the C1 of the ligand for binding of molecular oxygen, but the formation of the anthracycline-peroxide outside the active site cannot be excluded. It is noteworthy that the reaction with molecular oxygen in the active site of SwaQ2 may be required to ensure the correct regiochemistry at C1 and prevent the reaction at the chemically equivalent C11 position. Nonetheless, the single SDR enzyme is not sufficient for 1-hydroxylation as the peroxide is resolved into the anthracycline starting material and H_2O_2. For this reason, recruitment of polyketide cyclase-like SnoaL2 has been necessary to complete the reaction through stabilization of a resonance structure that prevents cleavage of H_2O_2. This process may have been facilitated by the relatively high stability of the anthracycline-peroxide, which can be detected by HPLC.[18] We propose that the intermediate may passively diffuse from the active site of SnoaW to SnoaL2 since no protein−protein interactions have been observed between the two proteins.[18]

The emergence of 1-hydroxylation has been highly important from an evolutionary perspective since the reaction has allowed an additional O-glycosylation site that is highly important for the biological activity of nogalamycin (**3**).[35] The complex chemical structures of anthracyclines precludes industrial manufacturing via organic synthesis.[1] For this reason, the characterization of the broad substrate specificity of the various 1-hydroxylases (Figure 1d and Figure 1e) is promising as it opens up possibilities to generate novel anthracycline congeners using metabolic engineering and combinatorial biosynthesis.[9]

MATERIALS AND METHODS

Bacterial Strains and Culture Conditions. *Escherichia coli* TOP10 (Invitrogen) was used for the cloning and production of the native enzymes and their mutants. Streptomyces strains used for the production of metabolites were cultivated in NoS-soyE1,[35] tryptone soya broth (TSB) (Oxoid), R2 yeast extract (R2YE), and mannitol soya flour medium (MS).[36] The *E. coli* TOP10 or BL21(DE3) (Merck) strains were cultivated in Luria−Bertrani or 2 × yeast extract/tryptone medium (2xTY). Ampicillin (100 μg/mL; Sigma-Aldrich) was used to cultivate *E. coli* TOP10, while kanamycin (50 μg/mL; Sigma-Aldrich) and apramycin (50 μg−1250 μg/mL; Sigma-Aldrich) were used for the cultivation of the *Streptomyces* strains.

Cloning and General DNA Techniques. The genes *snoaW* and *snoaL2* were obtained from previous studies.[18] *kstA15*, *kstA16, swaQ2, dvaQ2, virQ2,* and all mutants were ordered as DNA fragments with restriction enzyme recognition sites or cloned in a plasmid from either Thermo Fisher Scientific or GeneWiz. DNA-modifying enzymes and commercial kits used for digesting the DNA fragments and for recovering DNA from agarose gels were purchased from Thermo Fisher Scientific. The DNA fragments were digested with either BglII−HindIII or NcoI−HindIII restriction enzymes and cloned to the modified *pBAD*HisB-plasmid.[37] The constructs isolated after cloning were verified by sequencing (Eurofins MWG Operon).

For structure determination of KstA15 an expression construct with a removable N-terminal His_6-tag was used. The coding sequence of KstA15 was amplified by PCR using Pfu-Turbo polymerase (Agilent), appropriate amplification primers and subsequent cloning into pNIC28Bsa4 vector using ligation-independent cloning.[38] The construct contains an N-terminal hexahistidine tag and a tobacco etch virus (TEV) protease recognition site (MHHHHHHSSGVDLGTENLYFQ*S; an asterisk indicates the cut position) for affinity tag removal.

Production and Purification of Enzymes and Metabolites. The enzymes for enzymatic assays were produced in *E. coli* TOP10 as N-terminal hexahistidine-tagged recombinant proteins. The cells were cultured in 2 L bottles with 500−1000 mL of 2xTY at 30−37 °C with vigorous shaking until the OD_{600} reached ∼0.6 after which the cells were induced with 0.02% (w/v) L-arabinose. Protein production was carried out at 23 °C for 15−19 h. The cells were harvested by centrifugation and suspended in A-buffer pH 7.5 [50 mM sodium phosphate, 200 mM NaCl, 5 mM imidazole, and 10% (v/v) glycerol]. The cells were lysed by sonication, and the cell debris was removed by centrifugation. The soluble cell lysates were mixed with TALON Superflow (GE Healthcare) and incubated at 8 °C with gentle rotation for 30 min. The impurities were washed with A-buffer, and the target proteins were eluted from the column with B-buffer (A-buffer with 300 mM imidazole). The purity of the enzymes was analyzed with SDS PAGE. The enzymes were desalted with a PD-10 column (GE Healthcare) and stored at −20 °C in C-buffer pH 7.5 [100 mM sodium phosphate, 100 mM NaCl, 10% (v/v) glycerol] with glycerol added to 40% (v/v). The enzyme SnoaW was unstable and supplemented with 0.2% of octyl β-D-glucopyranoside (v/v).

For structural studies, the SwaQ2 DNA fragment was obtained from GeneWiz with an additional His-tag and a TEV protease site (MAHHHHHHHSSGVDLGTENLYFQ*S) and cloned to modified *pBAD*HisB-plasmid.[37] The protein was

https://doi.org/10.1021/acscatal.4c02623
ACS Catal. 2024, 14, 12359−12371

purified as mentioned above but with different buffers. D-buffer pH 8.0 [50 mM Tris/HCl, 200 mM NaCl, 10 mM imidazole, 10% (v/v) glycerol] was used for cell resuspension and washing of impurities, and E-buffer (D-buffer +300 mM imidazole) was used for eluting the protein. The eluted protein was desalted and recovered in F-buffer at pH 8.0 (25 mM Tris/HCl, 150 mM NaCl). TEV protease cleavage reaction was performed at 8 °C overnight in F-buffer (supplemented with 2 mM DTT) at a mass ratio of 1:100. The His_6-tagged TEV protease and the uncleaved tagged SwaQ2 proteins were removed by an immobilized metal ion affinity chromatography (IMAC). The flow-through containing the cleaved SwaQ2 was collected, desalted, and stored at −80 °C in F-buffer for crystallization.

For KstA15 crystallization, the His_6-tagged enzyme was expressed in *E. coli* BL21(DE3) at 21 °C. The cells were harvested by centrifugation (4,000 rpm x 30 min), resuspended in a buffer containing 25 mM Tris-HCl, 300 mM NaCl, 10 mM imidazole (pH 8.0), and lysed by the addition of lysozyme (40 μg/mL), DNase-I (6 μg/mL), $MgCl_2$ (1 mM), and sonication. The clarified lysate was loaded onto a 1 mL Ni-NTA column (Thermo Scientific), washed with 20 column volume of 25 mM Tris-HCl, 300 mM NaCl, and 10 mM imidazole (pH 8.0), and the His-tagged proteins were eluted by an increasing imidazole gradient (25−500 mM). The target protein-containing fractions were pooled, and imidazole was removed by passing through a PD10 desalting column (GE Healthcare) that retained the proteins in 25 mM Tris and 150 mM NaCl (pH 8.0). For affinity tag-removal, protein preparations were treated with TEV protease (5 μg/mg target protein) in the presence of 2 mM DTT at 20 °C for 18 h. The His-tagged TEV protease and uncleaved proteins were removed by running the samples through a 1 mL Ni-NTA column, collecting the processed, tag-free proteins in the flow-through. The resulting fractions were concentrated using a Vivaspin device (Sartorius) with 10 kDa molecular weight cutoff to <2 mL and loaded on size exclusion chromatography columns (Superdex-200 or −75, GE Healthcare), equilibrated by 25 mM Tris and 150 mM NaCl (pH 8.0). Peak fractions of the recombinant proteins or protein complexes were pooled and concentrated using a Vivaspin device with 10-kDa cutoff filters to 21 mg/mL. The purified recombinant proteins were analyzed in SDS-PAGE (Figure S11). The protein preparations were either used immediately for crystallization and follow-up experiments or aliquoted, flash frozen in liquid N_2, and stored at −80 °C.

For the metabolites, the strain *S.albus*/pSnoΔaW was used for the production of the 3′,4′-demethoxy-nogalose-nogalamycinone substrate (**7**), while the strain *S.albus*/pSnoΔgE was used for the production of the nogalamycinone substrate (**5**). Both strains were generated in previous studies.[35] Aclacinomycin T (**8**) and aklavinone (**6**) were obtained by the acid hydrolysis of commercial aclacinomycin A. Doxorubicin and daunorubicin are commercially available.

Protein Crystallization and Structure Determination. Crystals of SnoaL2 with bound polyketide compounds were produced at 20 °C using the vapor diffusion method in 24-well cell culture plates (Sarstedt, REF:83.3922, Sarstedt AG and Co. KG, Numbrecht, Germany, EU) by mixing 1.5 μL of protein solution at 24 mg/mL containing 2.0 mM of **7** or **9** (in the buffer 25 mM Tris-HCl 150 mM NaCl pH 8.0) with 1.5 μL of the well solution (0.1 M MES pH 6.5/0.2 M MgCl2/25% PEG3350). The crystals for data collection were picked in nylon loops (Hampton) and were flash frozen and stored in liquid nitrogen until data collection.

The SwaQ2 complex was crystallized at 21 mg/mL protein concentration in the presence of 5 mM NADPH and 1.5 mM doxorubicin (**2**) at 20 °C. The sitting drops were set up using the Mosquito crystallization robot by mixing 0.15 μL of protein solution and 0.15 μL of crystallization buffer (0.1 M Na-cacodylate pH 6.67, 1.0 M Na_3-citrate). The dark orange crystals were dipped in a drop composed of 25% glycerol/1.2 M Na_3-citrate for cryoprotection, flash frozen in litho loops (MiTeGen, Ithaca, NY, USA), and stored in liquid nitrogen until data collection.

Crystals of KstA15 were produced at 20 °C using the vapor diffusion method in 24-well cell culture plates (Sarstedt, REF:83.3922, Sarstedt AG and Co. KG, Numbrecht, Germany, EU) by mixing 1 μL of protein solution at 21 mg/mL (in the buffer 25 mM Tris-HCl, 150 mM NaCl pH 8.0, containing **9** at 2 mM) with 2 μL of the well solution (0.1 M Bis-TRIS-propane pH 7.75/2.2 M ammonium sulfate). The crystals for data collection were picked in litho loops (Mitigen) dipped in a drop of the crystallization buffer containing 25% glycerol for cryoprotection, flash frozen, and stored in liquid nitrogen until data collection.

X-ray diffraction data sets for the **7** or **9** complexes of SnoaL2 and the data set for the apo-KstA15 were collected at the ID23−2 beamline at the ESRF (Grenoble, France, EU) to 1.80, 2.00, and 2.1 Å resolution, respectively. The crystal characterization and data collection parameters were based on EDNA,[39] and diffraction data were indexed and integrated using XDS[40] and scaled by AIMLESS from the CCP4i suite.[41] The X-ray data set for the SwaQ2 complex crystal was collected at the BioMAX beamline[42] of the MAX-IV synchrotron (Lund, Sweden, EU), and the data were indexed and integrated by AutoProc[43] and scaled by AIMLESS from the CCP4i suite.[41] X-ray diffraction data statistics are summarized in Table S2.

The structures of KstA15 and the two SnoaL2 polyketide complexes were solved by molecular replacement using MOLREP[44] in the space group $P2_12_12_1$ using the coordinates of the ligand-free SnoaL2 structure (PDB: 2GEX).[22] The structure of SwaQ2 was solved by molecular replacement employing PHASER[45] in the space group $P6_5$ with the coordinates of the homolog SimC7 from *Streptomyces antibioticus* (PDB: 5L3Z).[29]

The models were completed by manual model building in COOT[46] interspersed by crystallographic refinement by REFMAC-5.[47] Ligand refinement restrains were prepared by PRODRG.[48] The protein models were validated in COOT and by MOLPROBITY,[49] and figures were made in PyMOL (www.pymol.org). Refinement statistics and model parameters are summarized in Table S2. The crystallographic data were deposited with the Protein Data Bank under accession codes 8R2J, 8R2B, 8R2E, and 8R20.

Fluorescence-Based Ligand Binding Assay. The changes in the inherent fluorescence emission of the polyketides ligands were monitored in the absence or in the presence of the SwaQ2 in 96-well black plates (Costar 3694, Sigma-Aldrich) using the EnSpire Multilabel Reader (PerkinElmer) in the assay buffer 25 mM Tris-HCl, 150 mM NaCl, pH 7.5. The doxorubicin (**2**) at 25 μM were exposed to a concentration series of SwaQ2 in the range of 0−310 μM (exactly: 0, 4.8, 9.7, 19.4, 38.8, 77.5, 155.0, and 310.0 μM). The fluorescence emission was recorded using excitation spectrum at 470 nm and emission spectrum in 490−700 nm range with peak at 595 nm utilized in kinetic analysis. The fluorescence data were plotted using Origin (OriginLab, Northampton, Massachusetts, USA).

https://doi.org/10.1021/acscatal.4c02623
ACS Catal. 2024, 14, 12359−12371

Titration data of **2** with SwaQ2 were fit to the 1:1 binding model (Figure S3) that accounted for changes in the concentration of both reactants upon formation of the binary complex using the equilibrium titration routine of the Kintek Explorer software (KinTek Corporation, Austin, TX). The upper and lower bounds of the dissociation constant were calculated at a 10% increase in Chi2 over the minimal value using the FitSpace routine of the Kintek Explorer.

Enzymatic Reactions. The reactions were performed under aerobic and/or anaerobic conditions with either compound **1**, **2**, **5**, **6**, **7**, or **8** (Figures 1a–c) depending on the enzyme–substrate specificity. All reactions were carried out in 200 μL of reaction volume at room temperature (under aerobic conditions) or at 37 °C (under anaerobic conditions) with incubation time ranging from 5 to 60 min. The reaction products were analyzed by an SCL-10Avp HPLC with a SPD-M10Avp diode array detector (Shimadzu) using a Kinetex column (2.6 μm C18 100 Å, LC column 100 mm × 4.6 mm, Ea, Phenomenex) with a gradient from 15% acetonitrile containing 0.1% formic acid to 100%.

For the measurement of the SDR enzyme promiscuity based on the oxidation of NADPH, the reactions contained 120 μM substrate, 5 μM SDR-enzyme, and 500 μM NADPH. The formation of the dihydroquinone intermediates was monitored photometrically following the absorbance maxima of NADPH (340 nm) by UV/vis spectrophotometry.

The aerobic reactions mixture consisted of 150–200 μM substrates, 1–2 μM SDR enzymes (SnoaW, KstA16, SwaQ2, DvaQ2, VirQ2, and their mutants), 3–5 μM cyclase-like enzymes (SnoaL2, KstA15, AclR, CalR, and their mutants), and 0.5 mM NAD(P)H in reaction buffer (50 mM sodium phosphate, 50 mM NaCl [pH 7.5], 1.18%–1.27% DMSO [v/v]). The reactions were usually incubated for 5–60 min at 23 °C and then quenched by chloroform extraction. The chloroform phase containing the reaction products was dried and dissolved in methanol for HPLC analyses, as mentioned above. All the reactions were performed in triplicates.

The anaerobic reactions were carried out in 200 μL volume using either a Thunberg cuvette or in a whitley A35 anaerobic workstation (don whitley scientific), which is constantly filled with nitrogen. A day before the reactions were performed, the reaction buffers at different pH values containing spinning magnetic rods were kept overnight in an anaerobic glovebox in order to completely displace any oxygen in the buffers. On the following day, less than 15 μL of the substrates, cofactor, and enzymes (in 1.5 mL Eppendorf tubes) were kept opened for about 15 min in the anaerobic glovebox to remove any oxygen before the reactions were setup. The same concentrations of enzymes, substrates, and cofactor used under aerobic conditions were used in the anaerobic studies. The reactions were incubated for 1 h after which they were quenched by the addition of chloroform, and the compounds were extracted in chloroform. The chloroform was dried with a concentrator plus (Eppendorf) and dissolved with methanol. All the reactions were performed in triplicates. Analytical HPLC analyses were performed as described above.

Preparative Scale Enzymatic Synthesis of Product 11. In order to biosynthesize an adequate amount of compound **11** (Figure 6a) for NMR analysis, the reaction was carried out several times in 1–2 mL volumes in a Thunberg cuvette system under a nitrogen flux. The reaction mixture was analogous to that described for the aerobic reactions, with NADH introduced last, after all the oxygen had been flushed out with nitrogen (three flushes of 10 min, with vacuum applied in between). The enzymatic mutant SnoaL2 E106A was used to carry out the reaction, in partnership with SnoaW. The reactions were carried out for 1h at RT and quickly quenched with the addition of chloroform. The chloroform fraction was dried with a concentrator plus (Eppendorf) and dissolved with methanol. To finalize the purification, the samples were pooled and purified by preparative HPLC with a Shimadzu Nexera Prep HPLC system using a C18 5-μm, 10 × 250 mm SunFire (Waters) column at 2.5 mL/min, under the same gradient as described for the enzymatic reactions above.

Structure Determination of Enzymatic Reaction Products. The *in vitro* biosynthesized and purified **11** was extracted and dried. The sample was desiccated overnight and dissolved in deuterated methanol (eurisotop). Due to incomplete dissolution, some drops of DMSO-d_6 were added. Finally, the sample was filtered through glass wool to an NMR tube. The NMR was performed with a 500 MHz Bruker AVANCE-III NMR-system equipped with a liquid nitrogen-cooled Prodigy BBO (CryoProbe) or a 600 MHz Bruker AVANCE-III NMR-system equipped with a liquid nitrogen-cooled Prodigy TCI (inverted CryoProbe) at 298 K. The signals were internally referenced to the solvent signals or tetramethylsilane (TMS). The experiments included 1D (^{1}H) and 2D measurements (COSY, HMBC, and HSQC). Topspin (Bruker Biospin) was used for spectral analysis. Carbon chemical shifts were deduced from the HSQC and HMBC data.

The structure of compound **10** was confirmed by high-resolution electrospray ionization mass spectrometry by comparison of authentic standard **9**, which was converted to **10** using acid hydrolysis (Figure S10). High-resolution electrospray ionization mass spectra were recorded on Waters ACQUITY RDa Detector using a XBridge BEH C18 column, 130 Å, 5 μm, 4.6 × 30 mm (Waters) [method: solvent A: HO/0.1% HCOOH; solvent B: CH_3ON/0.1% HCOOH; flow rate: 0.8 mL/min; 0–2.20 min, 2–100% B; 2.20–2.50 min, 100% B; 2.50–2.80 min, 100–2% B; 2.80–3.00 min, 2% B].

Molecular Docking of Compounds 11 and 12. The 3D structures of compounds **11** and **12** were created via Chem3D software, with MM2 energy minimization (Table S3). In the case of compound **12**, the sugar was manually rotated to a position similar to that of compound **7**. The structure of SnoaL2 in complex with **7** was used as the docking target, with the ligand removed. Docking was automated using the SwissDock web server.[50]

Bioinformatics. Anthracycline biosynthetic gene clusters (BGCs) were initially recovered from GenBank with BLAST[53] searches using the SnoaL sequence as query. The results were refined to identify gene clusters harboring 1-hydroxylase genes using MultiGeneBlast.[25] Multiple sequence alignment was carried out using ClustalOmega[51] and edited in ENDScript.[52]

■ ASSOCIATED CONTENT

Supporting Information

The Supporting Information is available free of charge at https://pubs.acs.org/doi/10.1021/acscatal.4c02623.

Phylogenetic analysis, enzymatic assays, HPLC and NMR analyses of substrates and products, X-ray diffraction data and refinement statistics, and molecular modeling. Accession Codes: Crystallographic data have been deposited with the Protein Data Bank under accession codes 8R2J, 8R2B, 8R2E, and 8R20 (PDF)

https://doi.org/10.1021/acscatal.4c02623
ACS Catal. 2024, 14, 12359–12371

AUTHOR INFORMATION

Corresponding Authors

Robert Schnell − *Assoc. Prof R. Schnell−Department of Neuroscience, Karolinska Institutet, Stockholm SE-17177, Sweden; Department of Molecular Neurosciences, Center for Brain Research, Medical University of Vienna, Vienna A-1090, Austria;* orcid.org/0000-0001-7530-3629; Email: robert.schnell@ki.se

Mikko Metsä-Ketelä − *Prof. M. Metsä-Ketelä−Department of Life Technologies, University of Turku, Turku FIN−20014, Finland;* orcid.org/0000-0003-3176-2908; Email: mianme@utu.fi

Authors

Benjamin Nji Wandi − *Prof. M. Metsä-Ketelä−Department of Life Technologies, University of Turku, Turku FIN−20014, Finland;* orcid.org/0000-0003-1071-3111

Pedro Dinis − *Prof. M. Metsä-Ketelä−Department of Life Technologies, University of Turku, Turku FIN−20014, Finland*

Vilja Siitonen − *Prof. M. Metsä-Ketelä−Department of Life Technologies, University of Turku, Turku FIN−20014, Finland*

Gunter Schneider − *Prof. em. G. Schneider−Department of Medical Biochemistry and Biophysics, Karolinska Institutet, Stockholm SE-17177, Sweden*

Complete contact information is available at: https://pubs.acs.org/10.1021/acscatal.4c02623

Author Contributions

The manuscript was written through contributions of all authors. All authors have given approval to the final version of the manuscript.

Notes

The authors declare no competing financial interest.

ACKNOWLEDGMENTS

The authors wish to acknowledge the Academy of Finland (Grant nr: 340013 and 354998 to MM-K) and the Swedish Research Council (Grant nr: 2018-03999 to G.S. and R.S.) for funding. We acknowledge the Protein Science Facility at Karolinska Institutet, Turku Protein Core at University of Turku, the beamline staff of the Biomax beamline at the MAX-IV synchrotron facility (Lund, Sweden), and the ID23-2 beamline at the European Synchrotron Radiation Facility (Grenoble, France). We thank Georgi Belogurov for his help in the kinetic analysis of SwaQ2-doxorubicin interactions and Eric. S. Nybo for critical reading of the manuscript.

REFERENCES

(1) Hulst, M. B.; Grocholski, T.; Neefjes, J. J. C.; van Wezel, G. P.; Metsä-Ketelä, M. Anthracyclines: Biosynthesis, Engineering and Clinical Applications. *Nat. Prod. Rep.* **2022**, *39* (4), 814−841.

(2) Metsä-Ketelä, M.; Niemi, J.; Mäntsälä, P.; Schneider, G. Anthracycline Biosynthesis: Genes, Enzymes and Mechanisms. *Top. Curr. Chem.* **2008**, *282*, 101−140.

(3) Weiss, R. B. The Anthracyclines: Will We Ever Find a Better Doxorubicin? *Semin Oncol.* **1992**, *19* (6), 670−686.

(4) Elshahawi, S. I.; Shaaban, K. A.; Kharel, M. K.; Thorson, J. S. A Comprehensive Review of Glycosylated Bacterial Natural Products. *Chem. Soc. Rev.* **2015**, *44* (21), 7591−7697.

(5) van der Zanden, S. Y.; Qiao, X.; Neefjes, J. New Insights into the Activities and Toxicities of the Old Anticancer Drug Doxorubicin. *Febs J.* **2020**, *288* (21), 6095−6111.

(6) Pommier, Y.; Leo, E.; Zhang, H.; Marchand, C. DNA Topoisomerases and Their Poisoning by Anticancer and Antibacterial Drugs. *Chem. Biol.* **2010**, *17* (5), 421−433.

(7) Pang, B.; Qiao, X.; Janssen, L.; Velds, A.; Groothuis, T.; Kerkhoven, R.; Nieuwland, M.; Ovaa, H.; Rottenberg, S.; van Tellingen, O.; et al. Drug-Induced Histone Eviction from Open Chromatin Contributes to the Chemotherapeutic Effects of Doxorubicin. *Nat. Commun.* **2013**, *4* (1), 1908.

(8) Qiao, X.; van der Zanden, S. Y.; Wander, D. P. A.; Borras, D. M.; Song, J. Y.; Li, X.; van Duikeren, S.; van Gils, N.; Rutten, A.; van Herwaarden, T.; et al. Uncoupling DNA Damage from Chromatin Damage to Detoxify Doxorubicin. *Proc. Natl. Acad. Sci. U. S. A.* **2020**, *117* (26), 15182−15192.

(9) Nybo, S. E.; Brown, K. V.; Wandi, B. N.; Metsä-Ketelä, M. Pathway Engineering of Anthracyclines: Blazing Trails in Natural Product Glycodiversification. *J. Org. Chem.* **2020**, *85* (19), 12012−12023.

(10) Taube, H. Mechanisms of Oxidation with Oxygen. *J. Gen. Physiol.* **1965**, *49* (1), 29−50.

(11) Malmstrom, B. G. Enzymology of Oxygen. *Annu. Rev. Biochem.* **1982**, *51* (1), 21−59.

(12) Lindqvist, Y.; Koskiniemi, H.; Jansson, A.; Sandalova, T.; Schnell, R.; Liu, Z.; Mäntsälä, P.; Niemi, J.; Schneider, G. Structural Basis for Substrate Recognition and Specificity in Aklavinone-11-Hydroxylase from Rhodomycin Biosynthesis. *J. Mol. Biol.* **2009**, *393* (4), 966−977.

(13) Walczak, R. J.; Dickens, M. L.; Priestley, N. D.; Strohl, W. R. Purification, Properties, and Characterization of Recombinant Streptomyces sp. Strain C5 DoxA, a Cytochrome P-450 Catalyzing Multiple Steps in Doxorubicin Biosynthesis. *J. Bacteriol.* **1999**, *181* (1), 298−304.

(14) Siitonen, V.; Selvaraj, B.; Niiranen, L.; Lindqvist, Y.; Schneider, G.; Metsä-Ketelä, M. Divergent Non-Heme Iron Enzymes in the Nogalamycin Biosynthetic Pathway. *Proc. Natl. Acad. Sci. U. S. A.* **2016**, *113* (19), 5251−5256.

(15) Wandi, B. N.; Siitonen, V.; Palmu, K.; Metsä-Ketelä, M. The Rieske Oxygenase SnoT Catalyzes 2′′-Hydroxylation of l -Rhodosamine in Nogalamycin Biosynthesis. *ChemBiochem* **2020**, *21* (21), 3062−3066.

(16) Grocholski, T.; Koskiniemi, H.; Lindqvist, Y.; Mäntsälä, P.; Niemi, J.; Schneider, G. Crystal Structure of the Cofactor-Independent Monooxygenase SnoaB from Streptomyces Nogalater: Implications for the Reaction Mechanism. *Biochem.* **2010**, *49* (5), 934−944.

(17) Jansson, A.; Koskiniemi, H.; Erola, A.; Wang, J.; Mäntsälä, P.; Schneider, G.; Niemi, J. Aclacinomycin 10-Hydroxylase Is a Novel Substrate-Assisted Hydroxylase Requiring S-Adenosyl-L-Methionine as Cofactor. *J. Biol. Chem.* **2005**, *280* (5), 3636−3644.

(18) Siitonen, V.; Blauenburg, B.; Kallio, P.; Mäntsälä, P.; Metsä-Ketelä, M. Discovery of a Two-Component Monooxygenase SnoaW/SnoaL2 Involved in Nogalamycin Biosynthesis. *Chem. Biol* **2012**, *19* (5), 638−646.

(19) Fetzner, S.; Steiner, R. A. Cofactor-Independent Oxidases and Oxygenases. *Appl. Microbiol. Biotechnol.* **2010**, *86* (3), 791−804.

(20) Machovina, M. M.; Ellis, E. S.; Carney, T. J.; Brushett, F. R.; DuBois, J. L. How a Cofactor-Free Protein Environment Lowers the Barrier to O2 Reactivity. *J. Biol. Chem.* **2019**, *294* (10), 3661−3669.

(21) Grocholski, T.; Dinis, P.; Niiranen, L.; Niemi, J.; Metsä-Ketelä, M. Divergent Evolution of an Atypical S-Adenosyl-L-Methionine-Dependent Monooxygenase Involved in Anthracycline Biosynthesis. *Proc. Natl. Acad. Sci. U. S. A.* **2015**, *112* (32), 9866−9871.

(22) Beinker, P.; Lohkamp, B.; Peltonen, T.; Niemi, J.; Mäntsälä, P.; Schneider, G. Crystal Structures of SnoaL2 and AclR: Two Putative Hydroxylases in the Biosynthesis of Aromatic Polyketide Antibiotics. *J. Mol. Biol.* **2006**, *359* (3), 728−740.

(23) Sultana, A.; Kallio, P.; Jansson, A.; Wang, J. S.; Niemi, J.; Mäntsälä, P.; Schneider, G. Structure of the Polyketide Cyclase SnoaL Reveals a Novel Mechanism for Enzymatic Aldol Condensation. *Embo J.* **2004**, *23* (9), 1911−1921.

(24) Ma, H. M.; Zhou, Q.; Tang, Y. M.; Zhang, Z.; Chen, Y. S.; He, H. Y.; Pan, H. X.; Tang, M. C.; Gao, J. F.; Zhao, S. Y.; et al. Unconventional Origin and Hybrid System for Construction of Pyrrolopyrrole Moiety in Kosinostatin Biosynthesis. *Chem. Biol.* **2013**, *20* (6), 796−805.
(25) Medema, M. H.; Takano, E.; Breitling, R. Detecting Sequence Homology at the Gene Cluster Level with MultiGeneBlast. *Mol. Biol. Evol.* **2013**, *30* (5), 1218−1223.
(26) Räty, K.; Kantola, J.; Hautala, A.; Hakala, J.; Ylihonko, K.; Mäntsälä, P. Cloning and Characterization of Streptomyces Galilaeus Aclacinomycins Polyketide Synthase (PKS) Cluster. *Gene* **2002**, *293* (1−2), 115−122.
(27) Jörnvall, H.; Persson, B.; Krook, M.; Atrian, S.; Gonzalez-Duarte, R.; Jeffery, J.; Ghosh, D. Short-Chain Dehydrogenases/Reductases (SDR). *Biochemistry* **1995**, *34* (18), 6003−6013.
(28) Persson, B.; Kallberg, Y.; Bray, J. E.; Bruford, E.; Dellaporta, S. L.; Favia, A. D.; Duarte, R. G.; Jörnvall, H.; Kavanagh, K. L.; Kedishvili, N.; et al. The SDR (Short-Chain Dehydrogenase/Reductase and Related Enzymes) Nomenclature Initiative. *Chem. Biol. Interact.* **2009**, *178* (1−3), 94−98.
(29) Schäfer, M.; Le, T. B. K.; Hearnshaw, S. J.; Maxwell, A.; Challis, G. L.; Wilkinson, B.; Buttner, M. J. SimC7 Is a Novel NAD(P)H-Dependent Ketoreductase Essential for the Antibiotic Activity of the DNA Gyrase Inhibitor Simocyclinone. *J. Mol. Biol.* **2015**, *427* (12), 2192−2204.
(30) Campos-Martin, J. M.; Blanco-Brieva, G.; Fierro, J. L. G. Hydrogen Peroxide Synthesis: An Outlook beyond the Anthraquinone Process. *Angew. Chem., Int. Ed.* **2006**, *45* (42), 6962−6984.
(31) Zhang, Z.; Gong, Y. K.; Zhou, Q.; Hu, Y.; Ma, H. M.; Chen, Y. S.; Igarashi, Y.; Pan, L.; Tang, G. L. Hydroxyl Regioisomerization of Anthracycline Catalyzed by a Four-Enzyme Cascade. *Proc. Natl. Acad. Sci. U. S. A.* **2017**, *114* (7), 1554−1559.
(32) Skarka, A.; Škarydová, L.; Štambergová, H.; Wsól, V. Anthracyclines and Their Metabolism in Human Liver Microsomes and the Participation of the New Microsomal Carbonyl Reductase. *Chem. Biol. Interact.* **2011**, *191* (1−3), 66−74.
(33) Gui, C.; Chen, J.; Xie, Q.; Mo, X.; Zhang, S.; Zhang, H.; Ma, J.; Li, Q.; Gu, Y.-C.; Ju, J. CytA, a Reductase in the Cytorhodin Biosynthesis Pathway, Inactivates Anthracycline Drugs in Streptomyces. *Commun. Biol.* **2019**, *2* (1), 454.
(34) Fewer, D. P.; Metsä-Ketelä, M. A Pharmaceutical Model for the Molecular Evolution of Microbial Natural Products. *Febs J.* **2020**, *287* (7), 1429−1449.
(35) Siitonen, V.; Claesson, M.; Patrikainen, P.; Aromaa, M.; Mäntsälä, P.; Schneider, G.; Metsä-Ketelä, M. Identification of Late-Stage Glycosylation Steps in the Biosynthetic Pathway of the Anthracycline Nogalamycin. *ChemBiochem* **2012**, *13* (1), 120−128.
(36) Kieser, T.; Bibb, M.; Buttner, M.; Chater, K.; Hopwood, D. *Practical Streptomyces Genetics*; The John Innes Foundation: Norwich, 2000.
(37) Kallio, P.; Sultana, A.; Niemi, J.; Mäntsälä, P.; Schneider, G. Crystal Structure of the Polyketide Cyclase AknH with Bound Substrate and Product Analogue: Implications for Catalytic Mechanism and Product Stereoselectivity. *J. Mol. Biol.* **2006**, *357* (1), 210−220.
(38) Oke, M.; Carter, L. G.; Johnson, K. A.; Liu, H.; McMahon, S. A.; Yan, X.; Kerou, M.; Weikart, N. D.; Kadi, N.; Sheikh Md, A.; et al. The Scottish Structural Proteomics Facility: Targets, Methods and Outputs. *J. Struct. Funct. Genomics* **2010**, *11* (2), 167−180.
(39) Incardona, M.-F.; Bourenkov, G. P.; Levik, K.; Pieritz, R. A.; Popov, A. N.; Svensson, O. EDNA: A Framework for Plugin-Based Applications Applied to X-Ray Experiment Online Data Analysis. *J. Synchrotron Radiat.* **2009**, *16* (6), 872−879.
(40) Kabsch, W. Research Papers XDS Research Papers. *Acta Crystallogr. D Biol. Crystallogr.* **2010**, *66*, 125−132.
(41) Winn, M. D.; Ballard, C. C.; Cowtan, K. D.; Dodson, E. J.; Emsley, P.; Evans, P. R.; Keegan, R. M.; Krissinel, E. B.; Leslie, A. G. W.; McCoy, A.; et al. Overview of the CCP4 Suite and Current Developments. *Acta. Crystallogr. Section D. Biol. Crystallogr.* **2011**, *67* (4), 235−242.
(42) Ursby, T.; Hnberg, K. A.; Appio, R.; Aurelius, O.; Barczyk, A.; Bartalesi, A.; Bjelcic, M.; Bolmsten, F.; Cerenius, Y.; Doak, R. B.; et al. BioMAX − the first macromolecular crystallography beamline at MAX IV Laboratory. *J. Synchrotron Radiat.* **2020**, *27* (5), 1415−1429.
(43) Vonrhein, C.; Flensburg, C.; Keller, P.; Sharff, A.; Smart, O.; Paciorek, W.; Womack, T.; Bricogne, G. Data Processing and Analysis with the *AutoPROC* Toolbox. *Acta Crystallogr. D Biol. Crystallogr.* **2011**, *67* (4), 293−302.
(44) Vagin, A.; Teplyakov, A. Molecular Replacement with MOLREP. *Acta Crystallogr. D Biol. Crystallogr.* **2010**, *66* (1), 22−25.
(45) McCoy, A. J.; Grosse-Kunstleve, R. W.; Adams, P. D.; Winn, M. D.; Storoni, L. C.; Read, R. J. Phaser Crystallographic Software. *J. Appl. Crystallogr.* **2007**, *40* (4), 658−674.
(46) Emsley, P.; Lohkamp, B.; Scott, W. G.; Cowtan, K. Features and Development of Coot. *Acta Crystallogr. D Biol. Crystallogr.* **2010**, *66* (4), 486−501.
(47) Murshudov, G. N.; Skubák, P.; Lebedev, A. A.; Pannu, N. S.; Steiner, R. A.; Nicholls, R. A.; Winn, M. D.; Long, F.; Vagin, A. A. REFMAC5 for the Refinement of Macromolecular Crystal Structures. *Acta Crystallogr. D Biol. Crystallogr.* **2011**, *67* (4), 355−367.
(48) Schüttelkopf, A. W.; van Aalten, D. M. F. PRODRG: A Tool for High-Throughput Crystallography of Protein−Ligand Complexes. *Acta Crystallogr. D Biol. Crystallogr.* **2004**, *60* (8), 1355−1363.
(49) Williams, C. J.; Headd, J. J.; Moriarty, N. W.; Prisant, M. G.; Videau, L. L.; Deis, L. N.; Verma, V.; Keedy, D. A.; Hintze, B. J.; Chen, V. B.; et al. MolProbity: More and Better Reference Data for Improved All-Atom Structure Validation. *Protein Sci.* **2018**, *27* (1), 293−315.
(50) Grosdidier, A.; Zoete, V.; Michielin, O. SwissDock, a Protein-Small Molecule Docking Web Service Based on EADock DSS. *Nucleic Acids Res* **2011**, *39* (suppl), W270−W277.
(51) Sievers, F.; Wilm, A.; Dineen, D.; Gibson, T. J.; Karplus, K.; Li, W.; Lopez, R.; McWilliam, H.; Remmert, M.; Söding, J.; Thompson, J. D.; Higgins, D. G. Scalable Generation of High-Quality Protein Multiple Sequence Alignments Using Clustal Omega. *Mol. Syst. Biol.* **2011**, *7* (1), 539.
(52) Gouet, P.; Courcelle, E. ENDscript: A Workflow to Display Sequence and Structure Information. *Bioinform* **2002**, *18* (5), 767−768.
(53) Altschul, S. F.; Gish, W.; Miller, W.; Myers, E. W.; Lipman, D. J. Basic Local Alignment Search Tool. *J. Mol. Biol.* **1990**, *215* (3), 403−410.

https://doi.org/10.1021/acscatal.4c02623
ACS Catal. 2024, 14, 12359−12371